Experimental Investigations on Microshock Waves and Contact Surfaces

Yun Kai,[1,2,*] Walter Garen,[1] and Ulrich Teubner[1,2]

[1]*Hochschule Emden/Leer, University of Applied Sciences, Institute for Laser and Optics,*
Constantiaplatz 4, 26723 Emden, Germany
[2]*Carl von Ossietzky University of Oldenburg, Institute of Physics, 26111 Oldenburg, Germany*

The present work reports on progress in the research of a microshock wave. Because of the lack of a good understanding of the propagation mechanism of the microshock flow system (shock wave, contact surface, and boundary layer), the current work concentrates on measuring microshock flows with special attention paid to the contact surface. A novel setup involving a glass capillary (with a 200 or 300 μm hydraulic diameter D) and a high-speed magnetic valve is applied to generate a shock wave with a maximum initial Mach number of 1.3. The current work applies a laser differential interferometer to perform noncontact measurements of the microshock flow's trajectory, velocity, and density. The current work presents microscale measurements of the shock-contact distance L that solves the problem of calculating the scaling factor $Sc = Re \times D/(4L)$ (introduced by Brouillette), which is a parameter characterizing the scaling effects of shock waves. The results show that in contrast to macroscopic shock waves, shock waves at the microscale have a different propagation or attenuation mechanism (key issue of this Letter) which cannot be described by the conventional "leaky piston" model. The main attenuation mechanism of microshock flow may be the ever slower moving contact surface, which drives the shock wave. Different from other measurements using pressure transducers, the current setup for density measurements resolves the whole microshock flow system.

Shock waves are of interest in diverse disciplines in physics and technology (an overview is given in Refs. [1,2]). The related interests may be grouped as "large scale" and "small scale" research. Whereas large scale shock research with examples in astrophysics [3–5], aerospace technology [6,7], high energy density physics [8] (including inertial confinement fusion [9]), etc. is quite common, shock wave research at the small scale especially at the microscale ($<$ mm) is quite new to the scientific community. Examples are microshock channels [10], shock focusing [11], and medical applications [12,13].

In the last few decades, conventional shock tubes have been down scaled to perform the aforementioned small scale researches. In those cases, friction and heat conduction become non-negligible, which leads to deviation from classical theories. As a consequence, so-called scaling effects have become important. Down scaling normally means lowering the Reynolds number Re of the flow. In the experiments, this can normally be achieved by reducing either the initial pressure P_1 [14–17] or the hydraulic diameter D (or both parameters combined) [10,18–25]. These two different down scaling approaches may be regarded as equivalent [18], if the Reynolds number of the postshock flow Re_2 [18] or the scaling factor Sc [19] is the same.

Some works, such as Ref. [26], investigated microinstabilities in shock and particle acceleration. However, such work is related to shock thickness, not to the hydraulic diameter as here. Down scaling of D to the molecular level will change the physical description. However, the Knudsen number for our experimental conditions in atmospheric air is Kn $= \Lambda/D < 0.001$ (with $\Lambda \approx 68$ nm [27] as the mean free path, and $D = 200$ or 300 μm). Our Kn is also comparable with Ref. [28]. Hence, the current work is still related to continuum mechanics.

The current work concentrates on collisional shocks, namely, a situation where the shock thickness Δ is larger than Λ. For a shock wave with Mach number $M_s \approx 2$ in ambient air, there is $\Delta \approx 150$ nm; thus, $\Delta > \Lambda$ (smaller M_s corresponds to even larger values of Δ; details are given in Ref. [29]). The current work has to be distinguished from investigations on collisionless shocks, which are not subject to Coulomb collisions due to the large Λ.

Many aspects of microshock flows are still not understood, e.g., how long is the hot flow duration or named test time? How do they attenuate? Are they well described by existing theories and models? Thus, there is a demand for experiments on microshocks. Consequently, the current work intends to provide the experimental results. Furthermore, different from all other works in microshocks, the current work detects flow density by the use of laser differential interferometry (LDI) instead of pressure. Therefore, the current setup for density measurements resolves the whole microshock flow system. The thereby
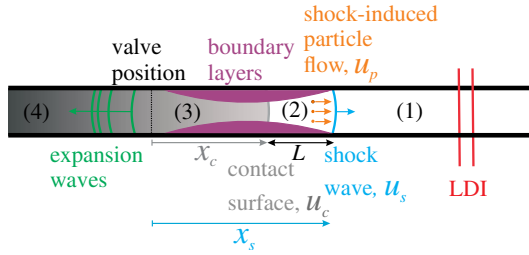
FIG. 1. A microshock flow in a capillary (simplified sketch). Region 1 is in front of the shock; region 2 is between the shock and the contact surface; region 3 is between the contact surface and the expansion fan (or waves); region 4 is the high pressure driver.

FIG. 2. Oscillograph traces (with normalized voltage) of the shock flows in the 200 μm capillary at the representative propagation distance x (coincides with the distance between the exit of the magnetic valve at position zero and LDI at x). The dash-dot line indicates the decreasing shock-induced density jump ρ_2/ρ_1. The photovoltage $U(t)$ scales with flow density $\rho(t)$.

obtained results help us to understand the propagation mechanism of microshock flows.

As shown in the simplified sketch in Fig. 1 (similar to Ref. [16]), a microshock flow can be divided into four regions (similar to a conventional shock tube). Every region corresponds to certain state variables such as pressure, flow velocity, density, temperature, etc. In this work, the state variables are indicated by subscripted indices according to the region (e.g., P_4 is the pressure of region 4). Square glass capillaries (CM Scientific) with hydraulic diameters of $D = 200$ and $300\ \mu$m are applied. The length of the $200\ \mu$m capillary is 300 mm, while the $300\ \mu$m capillary has a length of 600 mm. The capillary wall is half as thick as D of the corresponding capillary. A high-speed magnetic valve (Parker Hannifin) is applied to initiate the shock flow ($170 \pm 10\ \mu$s rise time, i.e., the time to open the valve completely, experimentally determined). The driver gas is helium with $P_4 = 8$ bar, while the driven gas is air at atmospheric pressure, i.e., 1 bar.

The flow in the capillary is investigated by LDI [30] (positioned successively at different distances x from the exit of the magnetic valve), which has been modified and applied for our earlier publications in Refs. [31–35]. The $1/e^2$ diameter of each interferometer beam inside the capillary is approximately $20\ \mu$m, i.e., much smaller than D. LDI is used in two different arrangements. These are (1) the "two beams in" arrangement with both beams passing through the capillary, which enables the time-of-flight method for a direct measurement of the shock wave velocity (see Fig. 1), and (2) the "one beam out" arrangement with only one beam passing through the capillary, and the other passing above the capillary. The latter arrangement is mainly intended for measuring the flow density and trajectory. The phase difference of the two interferometer beams results from the difference in the index of refraction, which correlates with the flow density via the Gladstone-Dale relation. As a result, the shock induced density jump ρ_2/ρ_1 can be deduced from the amplitude signal $U(t)$ detected by the photodiodes via $\rho_2/\rho_1 = \mathrm{asin}(U(t)/U_0)\lambda/(2\pi\kappa D) + 1$ (theory in Ref. [30]). $\lambda = 632.8$ nm is the wavelength of the applied HeNe laser, U_0 is the
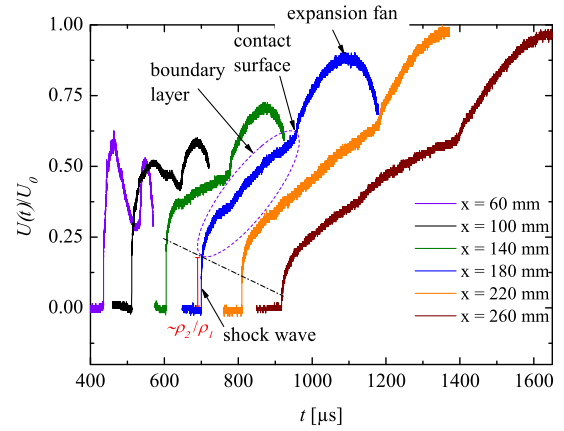
maximum photovoltage (normally between 2.6 and 2.8 V, affected by optical adjustment), and κ is the Gladstone-Dale constant; $\kappa = 2.93 \times 10^{-4}$ for atmospheric air [36]. Every experimentally determined value is an average value of five repetitions.

The experiments are multishot experiments. There is a shot-to-shot difference $< 20\ \mu$s (in the trajectory measurements), which is caused by, e.g., temperature fluctuation, the stability of the diagnostic, and the data reading uncertainty. This shot-to-shot difference (μs) is orders of magnitude smaller than the shock propagation time (ms); therefore, the reproducibility of our setup is very high. The error bars can be derived from the standard deviation resulting from the shot-to-shot difference and the system error (mainly by the length measurements of x). The error propagation in some values leads to bigger error bars, which are no more than 5% in general. The time instants of the shock and contact surface arrival are determined by reading the oscillographs either automatically (by MATLAB, using edge recognition) or manually (in the case of a very weak signal).

Figure 2 shows a selection of the oscillograph traces, measured at different x (regarded as the flow propagation distance, it is also the distance between the valve and LDI). Attenuation of the shock induced density jump is qualitatively noticeable (dash-dot line). The 100 MHz sampling rate of the oscilloscope provides the time resolution needed to allow the identification of different flow regions. Taking the curve at $x = 180$ mm as an example, one can first see a very sharp edge indicating the shock wave. The height of this edge correlates with ρ_2/ρ_1. After the passage of the shock wave, the voltage signal (and thus the density) increases slowly due to the growth of the boundary layer. Because the probe beam of LDI passes through the boundary layers and the core flow, it delivers the averaged
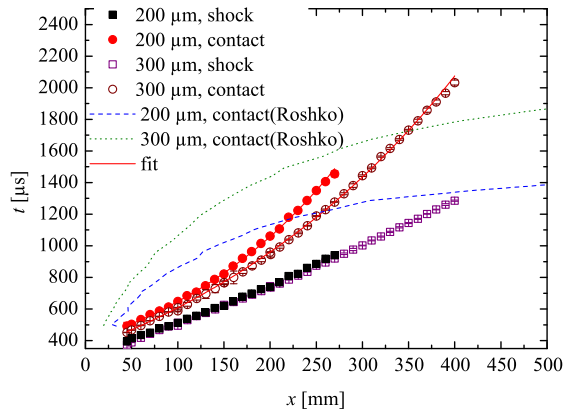
FIG. 3. The flow trajectories in the 200 and 300 μm diameter capillaries (from one beam out). Error bars derived from standard deviation are smaller than the symbols here. The theoretical model is from Roshko [15].

FIG. 4. Shock-contact distance L as a function of shock location x_s. L is derived from the shock wave and contact surface trajectories in Fig. 3 via the relation $L(x_s) = x_s(t) - x_{c,\text{fit}}(t)$.

flow density along its optical path. After further propagation, the contact surface shows up as the second edge (not as sharp as the first one). Then, the density continues to increase behind the contact surface, because of the arrival of the high density driver gas combined with the further growth of the boundary layer. Finally, the expansion fan (reflected from the valve bottom) arrives and decreases the flow density. Note that for curves at $x > 210$ mm, the expansion fan arrives much later; thus, they are outside of the working range of LDI.

As a preliminary result, the shapes of the oscillograph traces (which scale with density histories) are qualitatively consistent with Ref. [14]. But there are also significant differences shown by the following analysis.

Figure 3 shows the trajectories of the flow in the 200 and 300 μm capillaries, correspondingly.

(1) Shock wave. The shock waves trajectories in both capillaries only differ very slightly. Nevertheless, the slightly stronger bending of the 200 μm curve indicates that the shock wave in a smaller capillary experiences larger friction. The bending of the trajectories can be made clearer by differentiating the curve, i.e., using the two beams in arrangement of LDI to measure the local shock velocity. This will be shown later in Fig. 5.

(2) Contact surface. The curve of the 200 μm capillary is significantly above that of the 300 μm capillary. This means that the contact surface is moving faster in the larger tube.

The combination of points (1) and (2) shows that the down scaling has a significantly stronger impact on the contact surface than on the shock wave. The model from Roshko [15] does not agree with our measurements. In Ref. [15], the assumption of a thin boundary layer and $u_p = u_c$ are mainly applied. In the microshock flow, the boundary layer can be so thick that it fills more than half of the capillary cross section (approximated by using the Blasius equation in Ref. [37]). Moreover, u_p and u_c are not
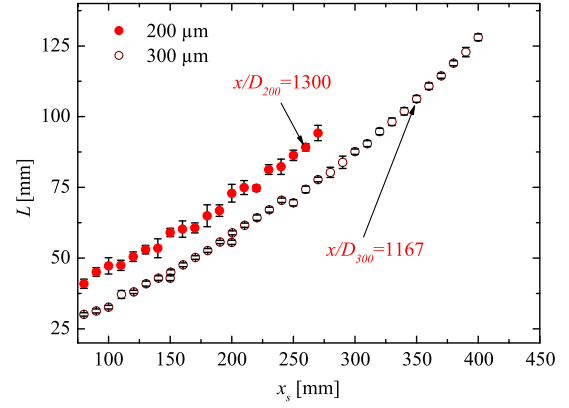
necessarily the same, because they correspond to two mechanisms: the postshock particles closely behind the shock wave are dragged into motion by the shock wave. On the other side, the contact surface is not "dragged" by the shock wave, but rather is "pushed" by the driver gas from behind. Therefore, Roshko's model does not apply for microshock flows.

When the calculation using directly measured data is inappropriate (in the sense that this introduces too large errors), it is quite common to represent the experimental data by an appropriate fit function prior to the calculations. Following this procedure, polynomial fits are applied for the contact surfaces in Fig. 3. The corresponding fit function is $x_{c,\text{fit}}(t) = a + b_1 t + b_2 t^2 + b_3 t^3$ (the horizontal and vertical axes are flipped for calculation convenience; the subscripts indicate the shock wave (s) and contact surface (c), respectively; a, b_1, b_2, and b_3 are fit parameters). This fit function is chosen for simple algebraic calculations in the following. L can thus be determined as $L(x_s) = x_s(t) - x_{c,\text{fit}}(t)$ (plotted in Fig. 4), where the $x_s(t)$ are the directly measured data from Fig. 3.

In the macroshock flow (experimental and theoretical) research [14,15,38], the contact surface and the shock wave eventually have the same speed leading to constant L (e.g., after the shock wave propagation of 230 times D in Ref. [14]). However, in the current work, the contact surface departs monotonically from the shock wave with increasing propagation distance. This is still the case after the propagation distance of 1300 times D, when the shock wave is slowed down and has the sound speed. Again, the thin boundary layers in macroscopic flows may be one of the causes of this disagreement.

The actual results may also be compared to the investigations in Ref. [19], in particular, to the scaling factor $Sc = Re \times D/(4L)$. Although in principle, down scaling has been successfully performed by applying this factor in different works such as Refs, [22,24,39], up to now the
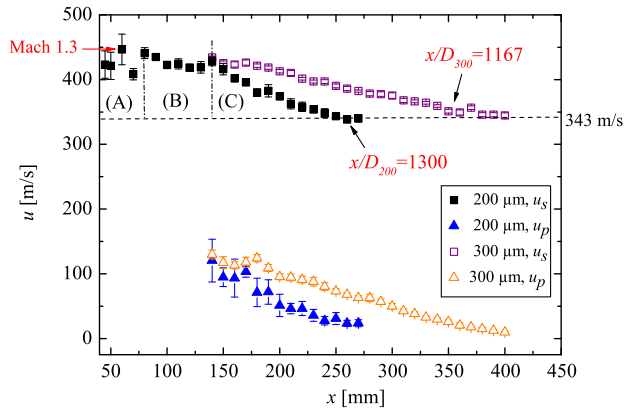
FIG. 5. Shock wave velocity u_s (direct measurement, two beams in) and postshock particle velocity u_p (indirect measurement) as functions of the propagation distance x.

main problem is still the missing knowledge of L (also considered as the friction length, but this could not be measured in Ref. [19]). It was only possible to use the shock propagation length x_s as a very rough approximation for L in those works. The current work, however, determines L and thus truly allows the calculation of the scaling factor. As an example, for $D = 200$ μm, the Reynolds number in front of the shock $Re = \rho_1 u_a D/\mu \approx 4300$ [with the atmospheric air density $\rho_1 \approx 1.205$ kg/m^3, dynamic viscosity $\mu \approx 1.82 \times 10^{-5}$ kg/(m s), sound velocity $u_a = 343$ m/s, and $41 \leq L \leq 89$ mm (corresponding to $80 \leq x \leq 260$ mm, phase B and C in Fig. 5)], the calculation yields $2.5 \leq Sc \leq 5.5$, which is part of the range discussed in Ref. [19]. This Sc range is expected to show dissipative effects.

Figure 5 shows the flow velocities. $u_s(x)$ is directly measured using the two beams in the arrangement of LDI.

The particle velocity u_p induced by the shock (immediately behind the shock front, see Fig. 1) can be derived from $u_p = u_s(1 - \rho_1/\rho_2)$ [2] by inserting the experimentally determined values u_s and ρ_2/ρ_1 (measured using the one beam out arrangement).

The initial shock velocity in Fig. 5 deviates from the existing theory on initial shock. For the case of a macroscopic shock tube operating at the same conditions (gas pairs and pressure ratio) as the microscopic tubes used here, the theoretical value of the shock Mach number is 1.9, which can be derived from the shock tube relation [2] and the Rankine-Hugoniot relations. Within the current work the initial shock Mach number is significantly lower, namely, 1.3 at maximum (see the arrow mark in Fig. 5) and later eventually turns into a sound wave. This is partially due to the rise time of the valve and partially due to the significant dissipative effects (wall friction and heat conduction) already happening in the early stage of shock formation. The dissipative effects on the initial shock Mach number are also reported in our previous work [35].

Indeed additional measurements (not shown here) with $D = 500$ and 700 μm capillaries, respectively, clearly show that the increasing dissipative effects (due to the increasing area-to-volume ratio) can be observed for decreasing D.

For the shock wave in the 200 μm capillary, u_s has three different phases: phase A shock formation (because trailing compression waves with large uncertainties are detected, not displayed in detail here); phase B changing shock attenuation followed by acceleration till the transition to the next phase; phase C quasilinear attenuation. The Reynolds number Re_2 of the particle flow immediately behind the shock (i.e., limited to the thin region where the boundary layer has not developed yet, as sketched in Fig. 1) can be calculated according to Refs. [18,35] as $Re_2 = u_p D\rho_2/\mu$. The calculations of Re_2 evidently show that the transition point between phase B and C correlates with the turbulent-laminar transition, because $Re_2 > 2300$ in phase B, while $Re_2 < 2300$ in phase C.

As described by the Moody diagram, the Reynolds number correlates with the Darcy friction factor λ [40]. For a turbulent flow one may use $\lambda = 0.3164/Re_2^{1/4}$, whereas $\lambda = 64/Re_2$ for laminar flow. At the turbulent-laminar transition, the friction is discontinuous. The sudden change from the larger λ at the turbulent side to the smaller one at the laminar side leads to a sudden friction reduction around the transition point (between $120 \leq x \leq 140$ mm in Fig. 5, 200 μm capillary). This explains the counterintuitive acceleration of the microshock wave in phase B (for additional information, see the Supplemental Material [41]).

In conclusion, the key issue of the current work is the experimental investigation of the propagation mechanism of the microshock flow. The main results may be summarized as follows.

1. The flow trajectory measurements show that the down scaling has a significantly stronger impact on the contact surface than on the shock wave itself.

2. The shock-contact distance L is measured. This measurement finally enables the calculation of the scaling factor Sc. Different from macroshock flows (with eventually constant L), L in microshock flows increases monotonically. The existing theories [14–16,38] thus need modifications.

Although not the key issue, a further result of observation is the shock acceleration in the flow transition phase (from the turbulent to the laminar regime).

Altogether, the present work yields a contribution to the understanding of the propagation mechanism of microshock flows from the aspect of the contact surface.

*Corresponding author.
 yun.kai@uni-oldenburg.de

[1] Y. Zel'dovich and Y. Raizer, *Physics of Shock Waves and High-Temperature Hydrodynamic Phenomena* (Courier Corporation, Mineola, New York, 2002).

[2] J. Anderson, *Modern Compressible Flow: With Historical Perspective* (McGraw-Hill, New York, 2003), Vol. 2.

[3] P. Moore and G. Hunt, *Atlas of the Solar System* (Rand McNally, Chicago, 1983).

[4] A. H. Sulaiman, A. Masters, M. K. Dougherty, D. Burgess, M. Fujimoto, and G. B. Hospodarsky, Phys. Rev. Lett. **115,** 125001 (2015).

[5] D. Schaeffer, D. Winske, D. Larson, M. Cowee, C. Constantin, A. Bondarenko, S. Clark, and C. Niemann, Phys. Plasmas **24,** 041405 (2017).

[6] A. Wagner, M. Schramm, J. Hickey, and K. Hannemann, Hypersonic shock wave boundary layer interaction studies on a flat plate at elevated surface temperature, in *22nd International Shock Interaction Symposium* (University of Glasgow, Glasgow, 2016).

[7] A. Russell, H. Zare-Behtash, and K. Kontis, J. Electrost. **80,** 34 (2016).

[8] E. Gamaly, L. Rapp, V. Roppo, S. Juodkazis, and A. Rode, New J. Phys. **15,** 025018 (2013).

[9] J. Lindl, Phys. Plasmas **2,** 3933 (1995).

[10] G. Mirshekari and M. Brouillette, J. Microelectromech. Syst. **21,** 739 (2012).

[11] T. Pezeril, G. Saini, D. Veysset, S. Kooi, P. Fidkowski, R. Radovitzky, and K. A. Nelson, Phys. Rev. Lett. **106,** 214503 (2011).

[12] K. Reddy and N. Sharath, Curr. Sci. **104,** 172 (2013).

[13] K. Takayama and T. Saito, Annu. Rev. Fluid Mech. **36,** 347 (2004).

[14] R. Duff, Phys. Fluids **2,** 207 (1959).

[15] A. Roshko, Phys. Fluids **3,** 835 (1960).

[16] H. Mirels, Phys. Fluids **6,** 1201 (1963).

[17] W. Garen, R. Synofzik, and A. Frohn, AIAA J. **12,** 1132 (1974).

[18] M. Sun, T. Ogawa, and K. Takayama, in *23th International Symposium on Shock Waves, Fort Worth, TX* (2001).

[19] M. Brouillette, Shock Waves **13,** 3 (2003).

[20] G. Mirshekari and M. Brouillette, Shock Waves **19,** 25 (2009).

[21] G. Mirshekari, M. Brouillette, J. Giordano, C. Hébert, J.-D. Parisse, and P. Perrier, J. Fluid Mech. **724,** 259 (2013).

[22] D. Zeitoun and Y. Burtschell, Shock Waves **15,** 241 (2006).

[23] D. Zeitoun, Phys. Fluids **27,** 011701 (2015).

[24] J. Austin and D. Bodony, Shock Waves **21,** 547 (2011).

[25] A. Deshpande and B. Puranik, Shock Waves **27,** 565 (2017).

[26] A. Marcowith, A. Bret, A. Bykov, M. E. Dieckman, L. O. Drury, B. Lembège, M. Lemoine, G. Morlino, G. Murphy, G. Pelletier *et al.*, Rep. Prog. Phys. **79,** 046901 (2016).

[27] S. Jennings, J. Aerosol Sci. **19,** 159 (1988).

[28] A. Deshpande and B. Puranik, Shock Waves **26,** 465 (2016).

[29] P. Thompson, *Compressible Fluid Dynamics* (McGraw-Hill, New York, 1971).

[30] G. Smeets, in *Proceedings of the 8th International Shock Tube Symposium* (1971).

[31] U. Teubner, Y. Kai, T. Schlegel, D. Zeitoun, and W. Garen, New J. Phys. **19,** 103016 (2017).

[32] Y. Kai, W. Garen, and U. Teubner, in *30th International Symposium on Shock Waves 2* (Springer, New York, 2017), pp. 1201.

[33] S. Udagawa, K. Maeno, I. Golubeva, and W. Garen, Shock Waves 1419 (2009).

[34] S. Udagawa, W. Garen, B. Meyerer, and K. Maeno, in *16th Australasian Fluid Mechanics Conference (AFMC)* (School of Engineering, The University of Queensland, 2007), pp. 207.

[35] W. Garen, B. Meyerer, S. Udagawa, and K. Maeno, Shock Waves 1473 (2009).

[36] H. Oertel, *Optische Strömungsmeßtechnik* (G. Braun, Karlsruhe, 1989).

[37] H. Schlichting and K. Gersten, *Boundary-layer theory* (Springer Science & Business Media, New York, 2003).

[38] W. Hooker, Phys. Fluids **4,** 1451 (1961).

[39] D. Ngomo, A. Chaudhuri, A. Chinnayya, and A. Hadjadj, Comput. Fluids **39,** 1711 (2010).

[40] E. Hering, R. Martin, and M. Stohrer, *Physik fuer Ingenieure* (Springer-Verlag, Berlin, 2007).

[41] See Supplemental Material at http://link.aps.org/supplemental/10.1103/PhysRevLett.120.064501 for details.